Electronic Supplementary Material (ESI) for Dalton Transactions.

Supporting Information

Copper complexes for the promotion of iminopyridine ligands derived from β-alanine and self-aldol additions: Magnetic behavior, relaxivity and cytotoxic properties.

Lucía Álvarez-Miguel,[a] Inés Álvarez-Miguel,[b] José M. Martín-Álvarez,[a] Celedonio M. Álvarez,[a] Guillaume Rogez,[c] Raúl García-Rodríguez,*[a] and Daniel Miguel*[a]

[a] GIR MIOMET-IU CINQUIMA/Química Inorgánica, Facultad de Ciencias, Universidad de Valladolid. Paseo de Belen 7, E-47011 Valladolid, Spain. E-mail: raul.garcia.rodriguez@uva.es, dmsj@qi.uva.es

[b] Instituto de Biología y Genética Molecular (IBGM). Universidad de Valladolid/CSIC, Sanz y Fores, 3, E-47003 Valladolid, Spain.

[c] Institut de Physique et Chimie des Matériaux de Strasbourg, UMR 7504 UdS-CNRS, 67034 Strasbourg Cedex 2, France.

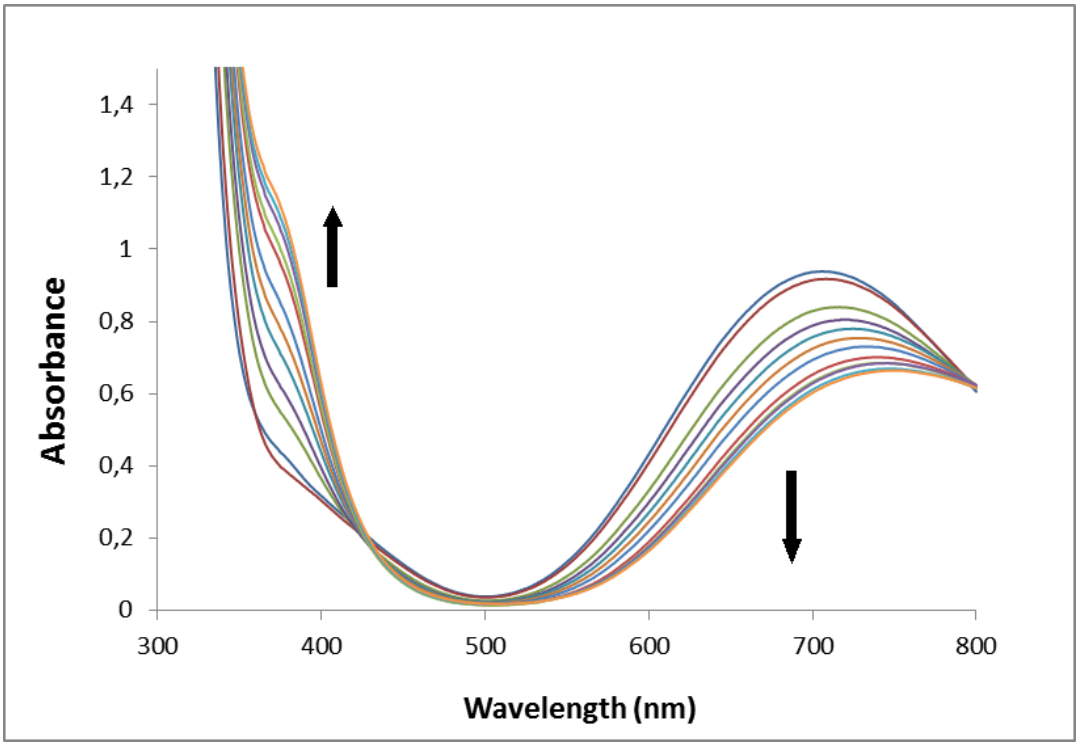

Figure S1: Absorption spectral changes of **5** (MeOH, 298 K, 510^{-3} M) upon the addition of HCl (MeOH, 298 K, 5×10^{-2} M). Depletion of the maximum at 712 nm is accompanied by the emergence of a new transition at 378 nm. The isosbestic point appears at 432 nm.

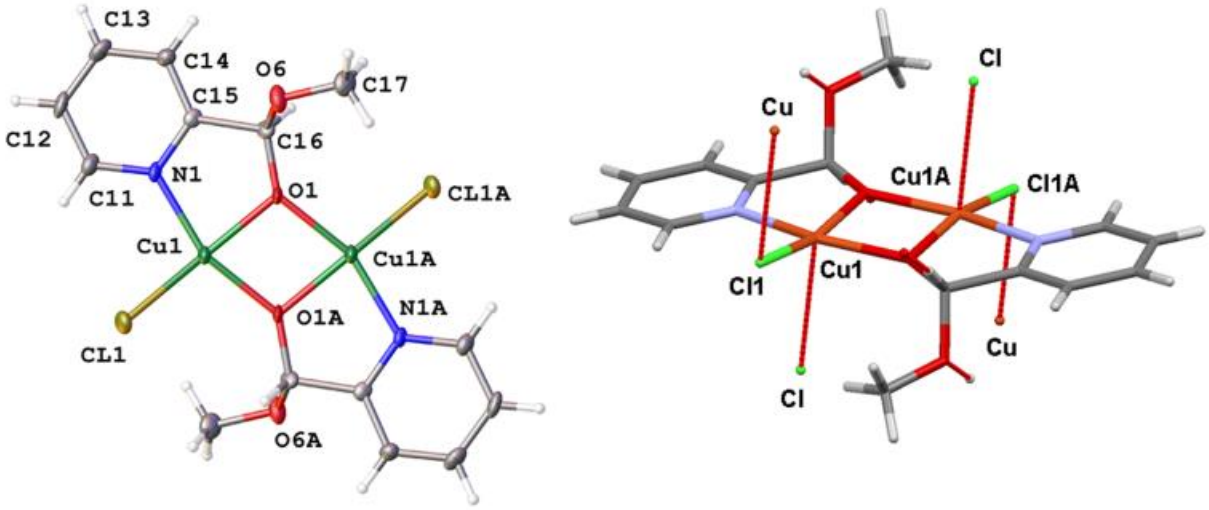

Figure S2: (Left) Perspective view of compound **7** showing the atom numbering. Selected bond distances (Å) and angles (°): Cu(1)-Cu(1A) 3.011(1), O(1)-O(1A) 2.433, Cu(1)-Cl(1) 2.229(1), Cu(1)-O(1) 1.940(3), Cu(1)-O(1A) 1.931(3), Cu(1)-N(1) 1.980(4), Cu(1)-O(1)-Cu(1A) 102.12(14), Cl(1)-Cu(1)-N(1) 98.94(11), N(1)-Cu(1)-O(1) 81.86(13), Cl(1)-Cu(1)-O(1A) 102.40(10), O(1)-Cu(1)-O(1A) 77.88(14). (Right) Perspective view of compound **7** showing the additional interactions. Selected bond distances (Å): Cu(1)-Cl 3.003

The XRD structure was published recently.[1]

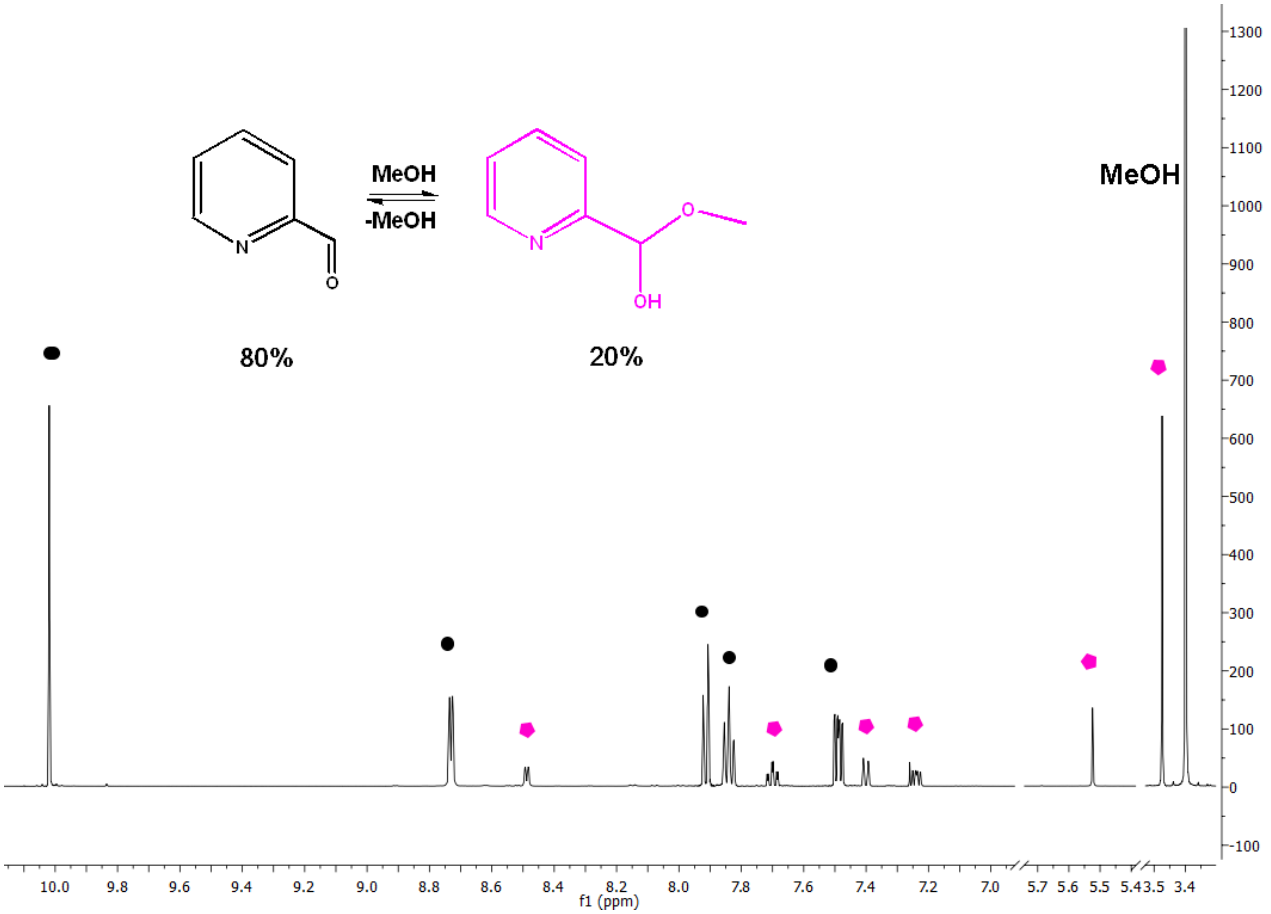

Figure S3: ^{1}H NMR spectrum of pyridine-2-carboxaldehyde with MeOH (1:1) in $CDCl_3$ showing formation of the hemiacetal.

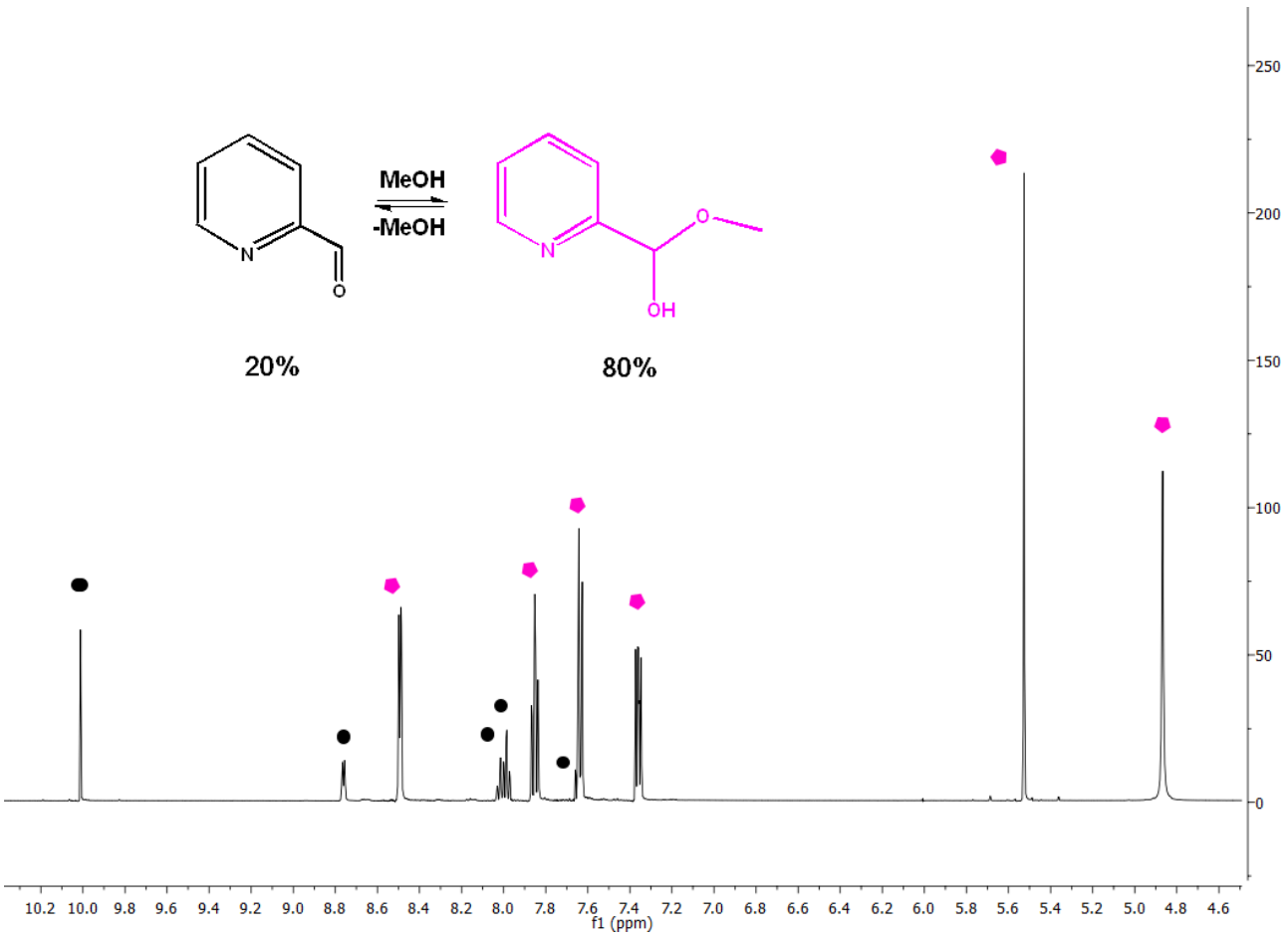

Figure S4: ^{1}H NMR spectrum of pyridine-2-carboxaldehyde in MeOD showing formation of the hemiacetal.

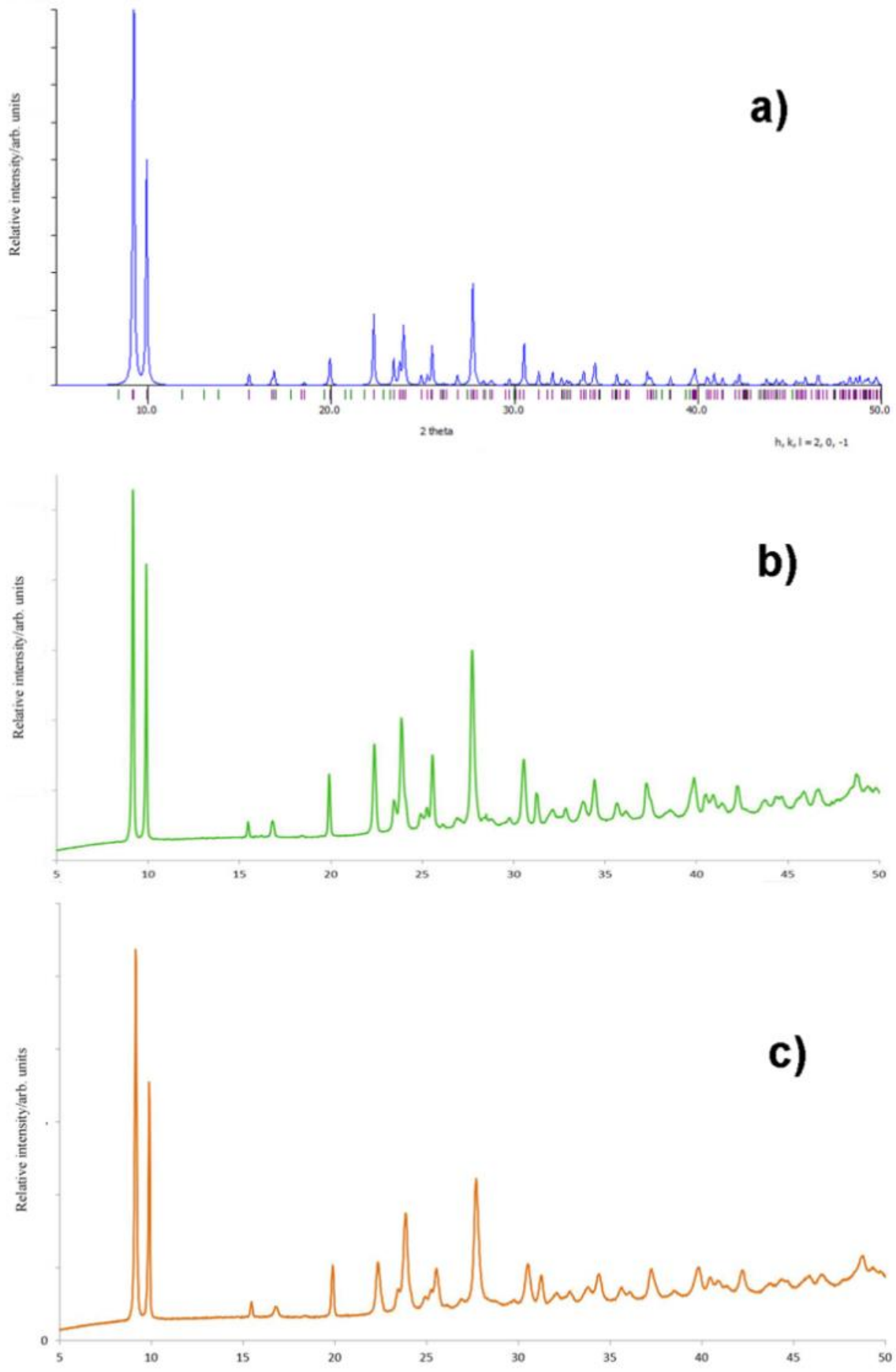

Figure S5. (a) XRPD analysis predicted from the single-crystal analysis of **7**. (b) Experimental XRPD analysis of the precipitate obtained from the reaction using CuCl. (c) Experimental XRPD analysis of the precipitate obtained from the reaction using $CuCl_2$.

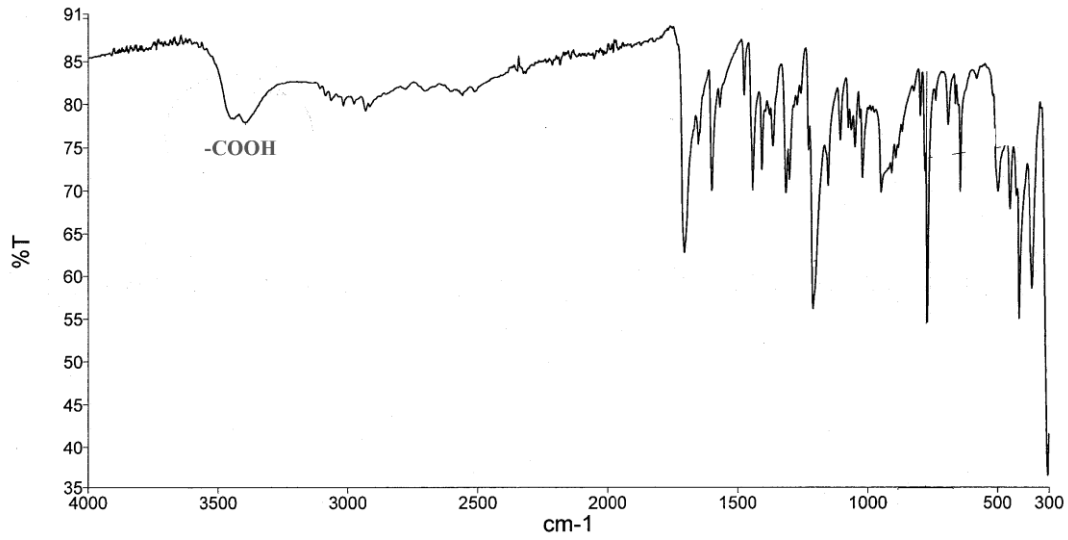

Figure S6: IR spectrum of complex **5**.

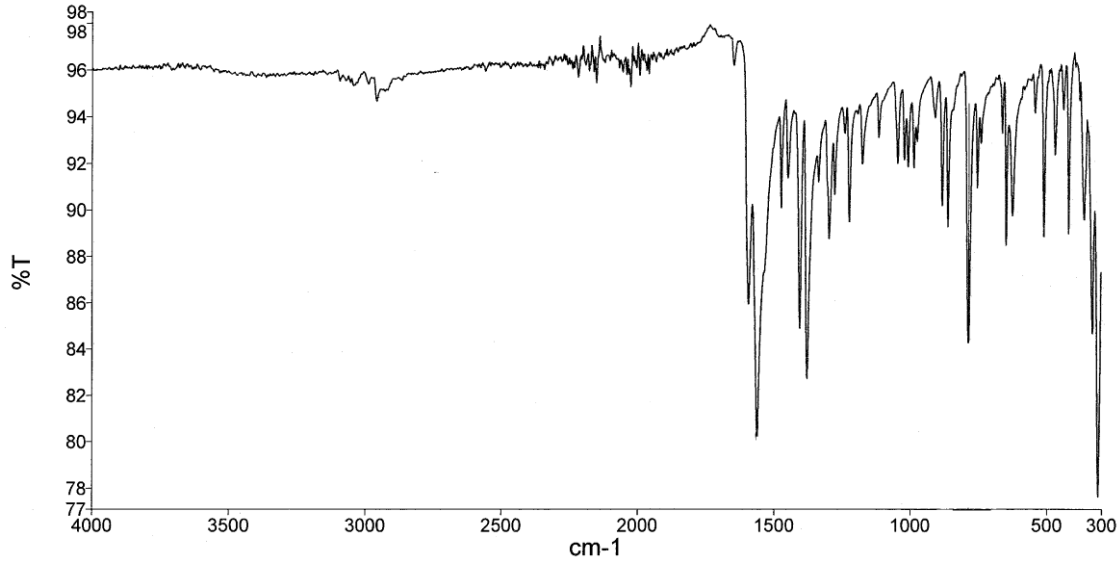

Figure S7: IR spectrum of complex **6**.

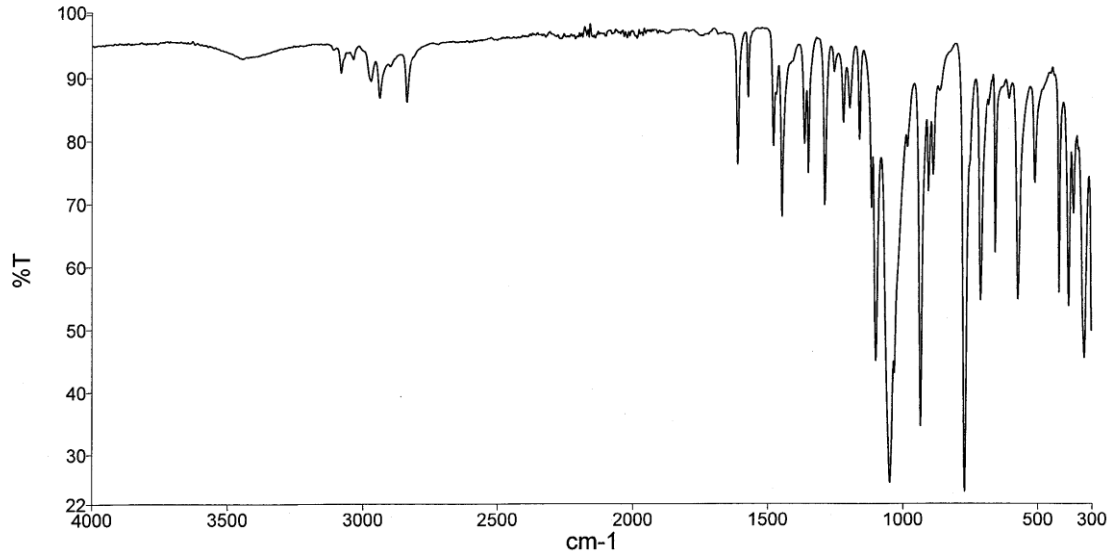

Figure S8: IR spectrum of complex **7**.

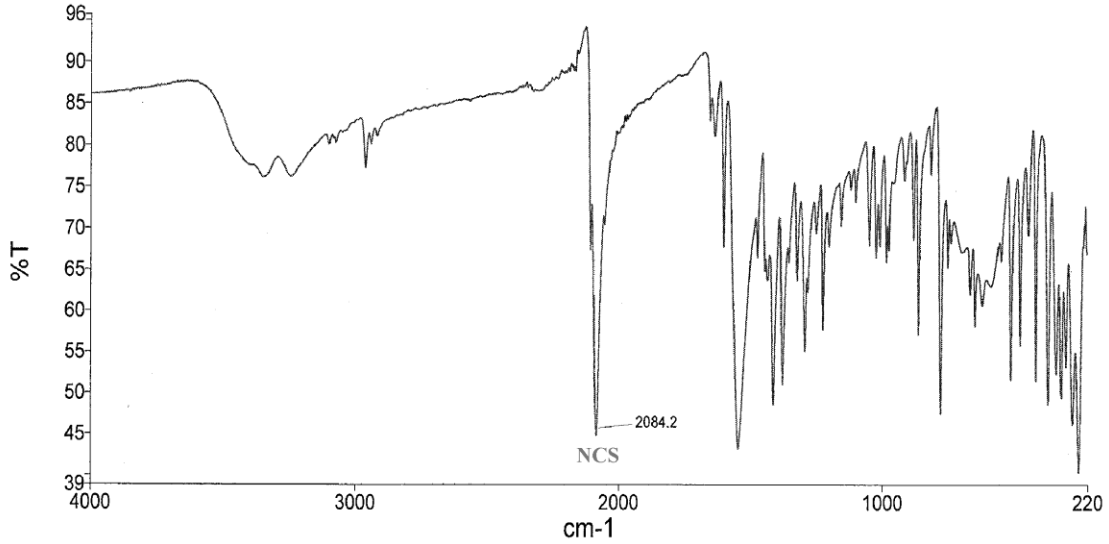

Figure S9: IR spectrum of complex **9**.

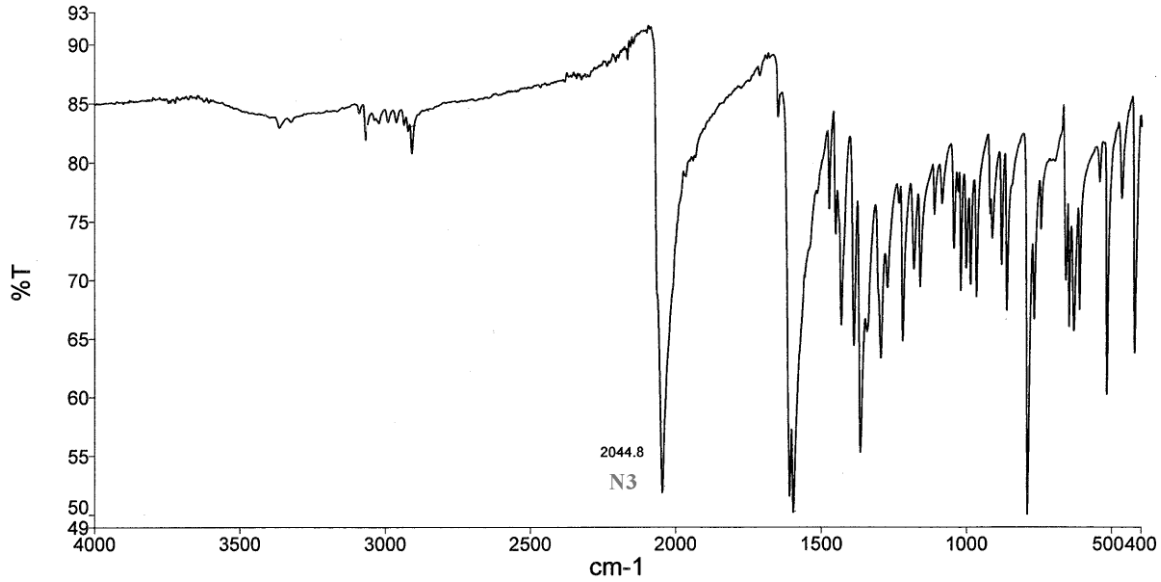

Figure S10: IR spectrum of complex **10a** (zigzag extended structure)

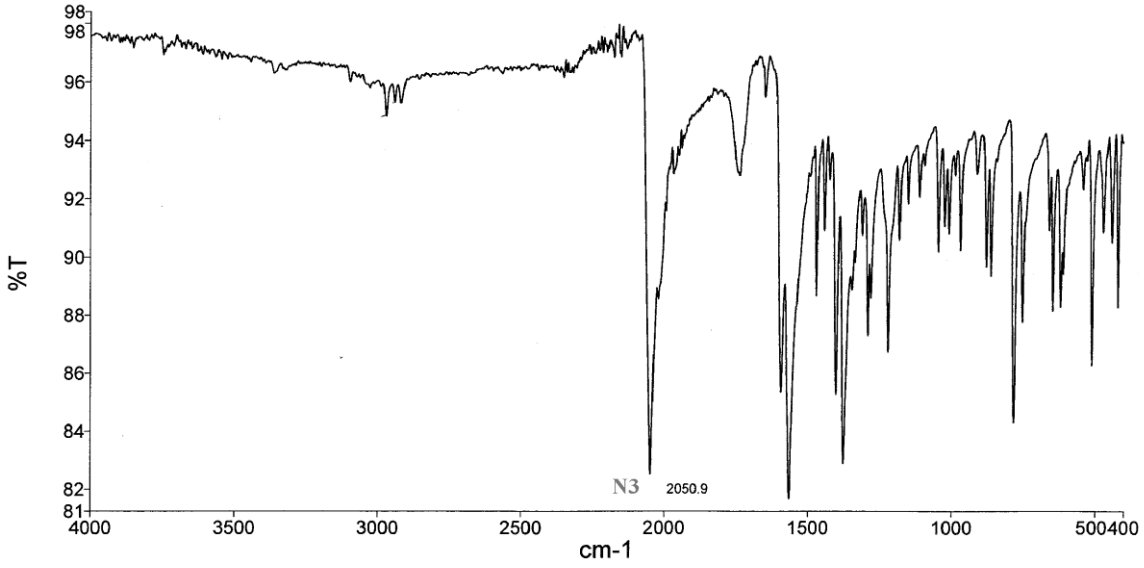

Figure S11: IR spectrum of complex **10b**

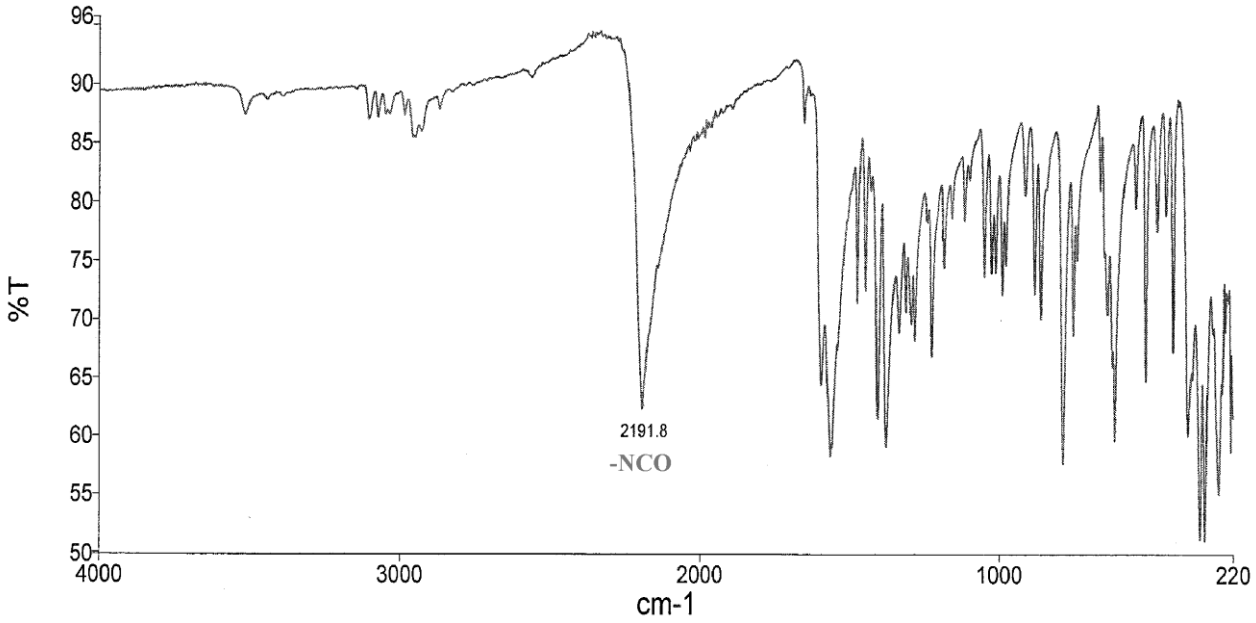

Figure S12: IR spectrum of complex **11**.

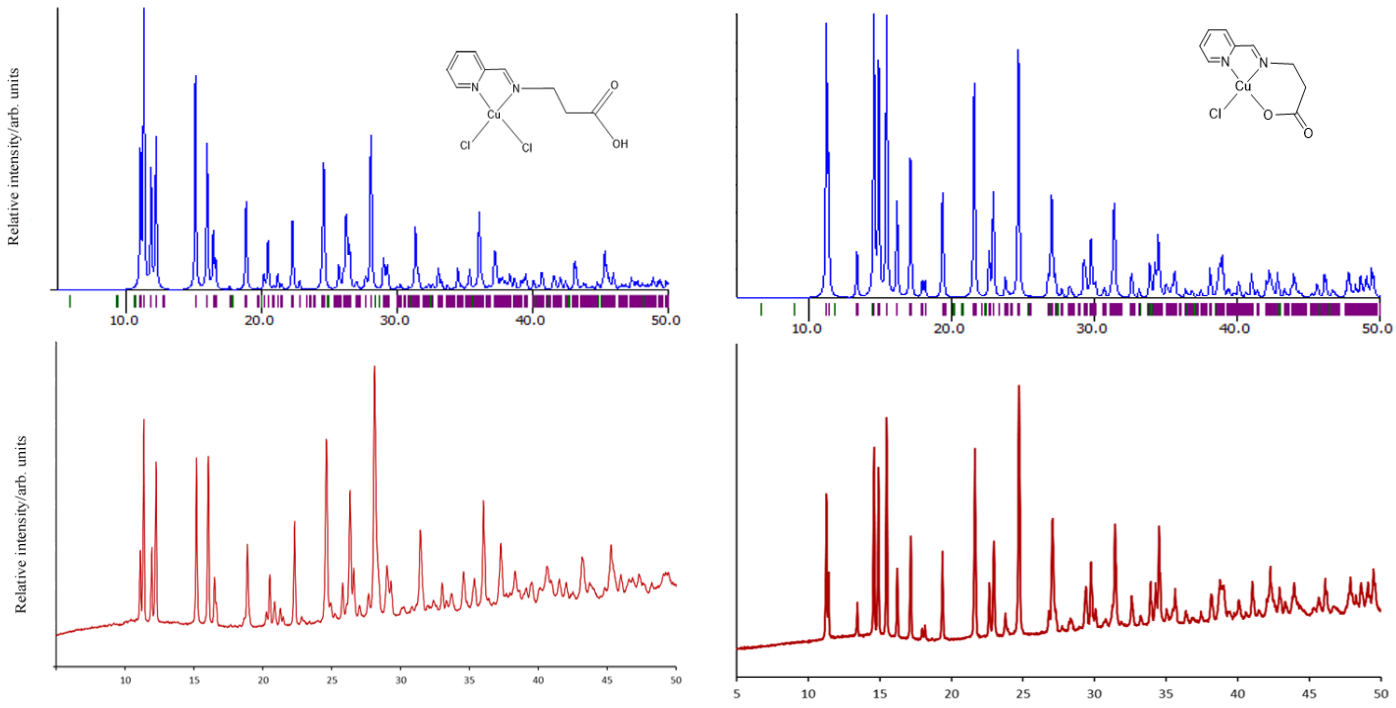

Figure S13: Comparison of the predicted (above, blue) and experimental XPRD patterns (below, red) for compounds **5** and **6**, respectively.

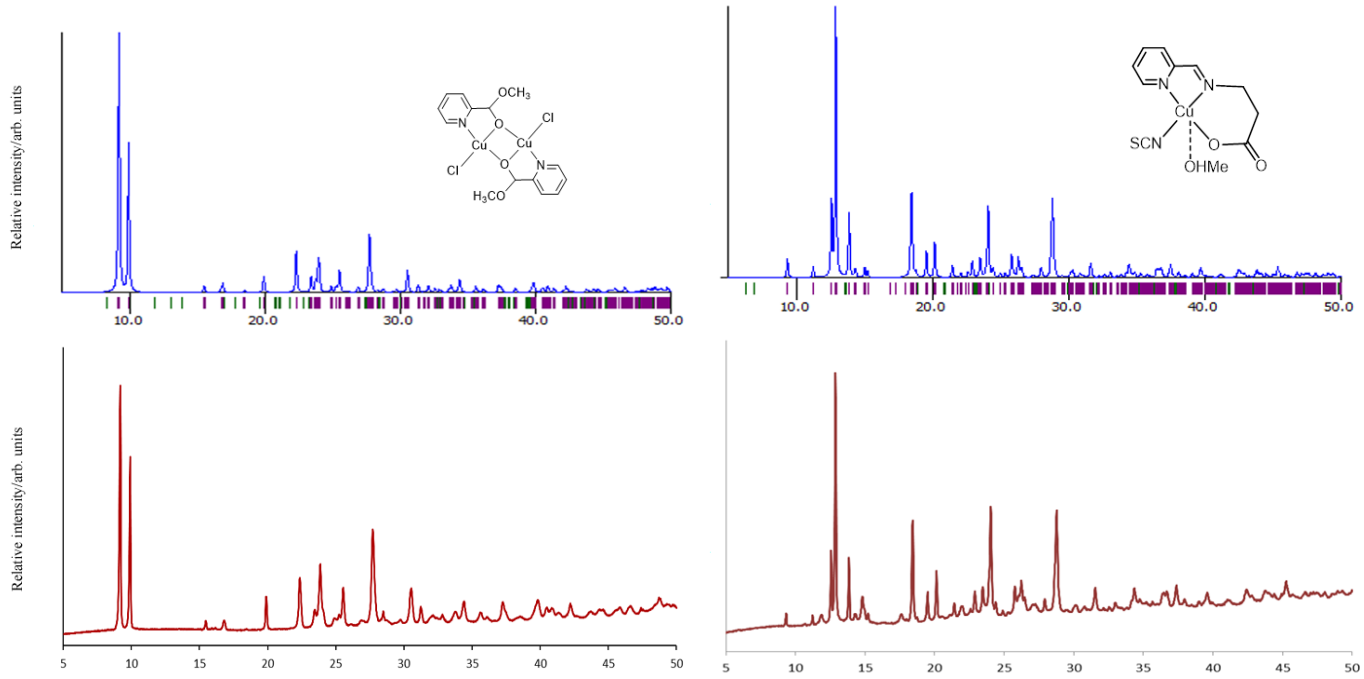

Figure S14: Comparison of the predicted (above, blue) and experimental XPRD patterns (below, red) for compounds **7** and **9**, respectively

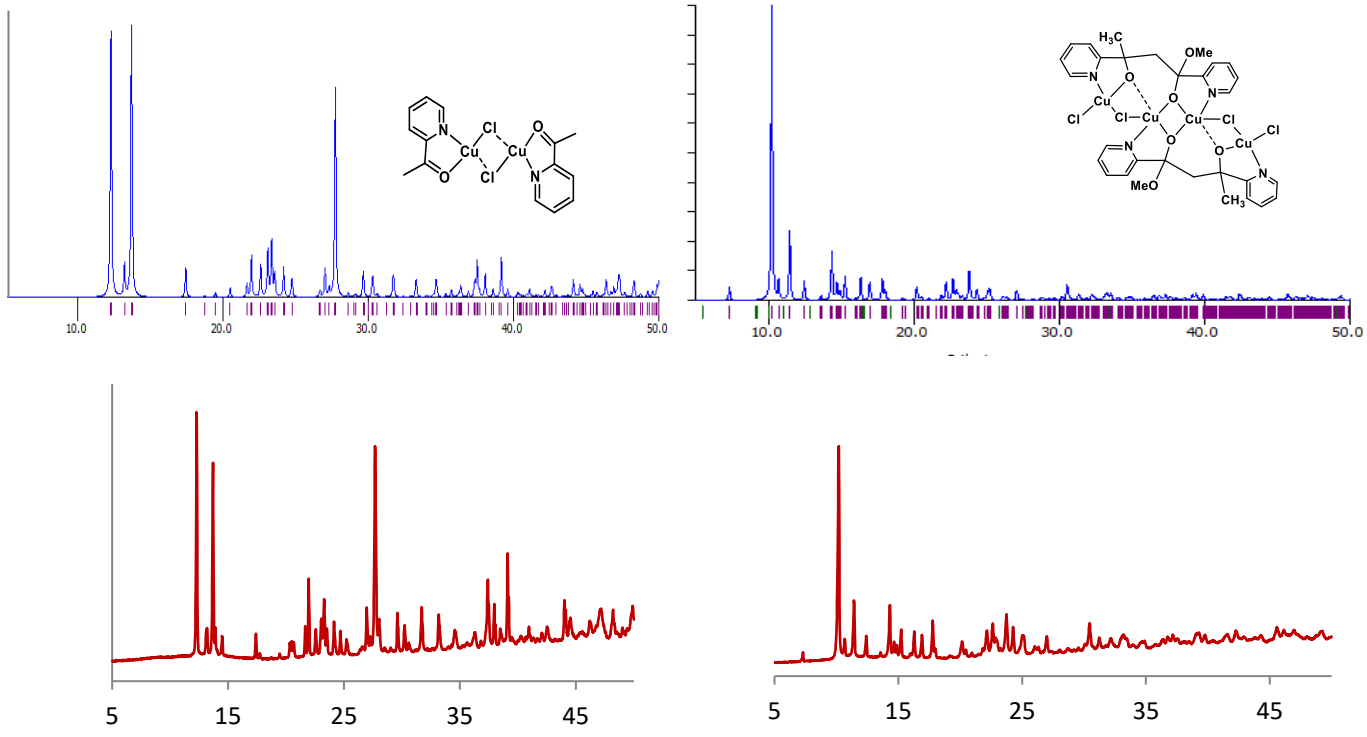

Figure S15: Comparison of the predicted (above, blue) and experimental XPRD patterns (below, red) for compounds **2b** and **8**, respectively

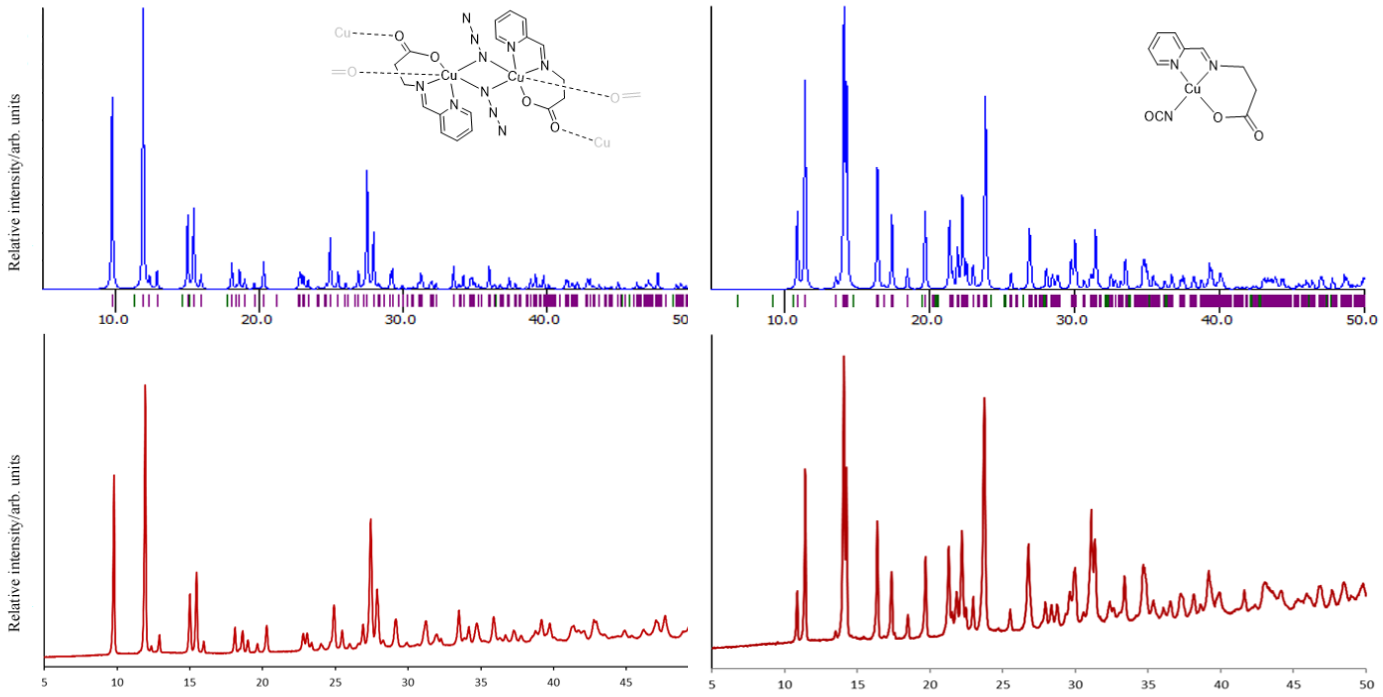

Figure S16: Comparison of the predicted (above, blue) and experimental XPRD patterns (below, red) for compounds **10b** and **11**, respectively

Magnetic Measurements

The magnetic properties of the copper complexes **5**, **6**, **7**, **9**, **10b** and **11** were investigated in the temperature range 1.8-300 K at a magnetic field of 5000 G. The corresponding Curie constant C and Weiss temperature θ were determined from the high-temperature (above 100 K) fit of the inverse susceptibility using the Curie-Weiss law (Table 1 in the paper).

Compound 7

7 presents a strongly antiferromagnetic coupling (Figure S18). The data (χT and χ) were fit simultaneously using the following spin Hamiltonian, where all parameters have their usual meaning and the spin operator S is defined as:

$S = SCu_1 + SCu_2$

$H = -J\ SCu_1\ SCu_2 + g\ \beta\ H\ S$

To reproduce the data satisfactorily, we had to consider a certain amount ρ of paramagnetic impurity (S_{impur} = ½). The fitting gave the following values: J = -433(1) cm^{-1}, g = 2.18(1) and ρ = 0.4(1)%, with an excellent agreement factor R = 5×10-7, where R is defined as $\sum(\chi T_{obs} - \chi T_{calc})^2/\sum(\chi T_{obs})^2$.

The very large value of J indicates very strong antiferromagnetic coupling between the copper (II) centers, which occurs via a superexchange mechanism through the oxo-bridges. It has been demonstrated that the value, sign and magnitude of the exchange interaction through the oxygen bridge in oxo-bridged Cu (II) dimers is strongly dependent on the angle Cu(1)-O-Cu(1A), the nature of the terminal ligands and the distortions of the coordination geometry. The calculated value of -433 cm^{-1} for the exchange interaction is consistent with the Cu(1)-O-Cu(1A) angle of 102.40° found in the solid-state structure.[2]

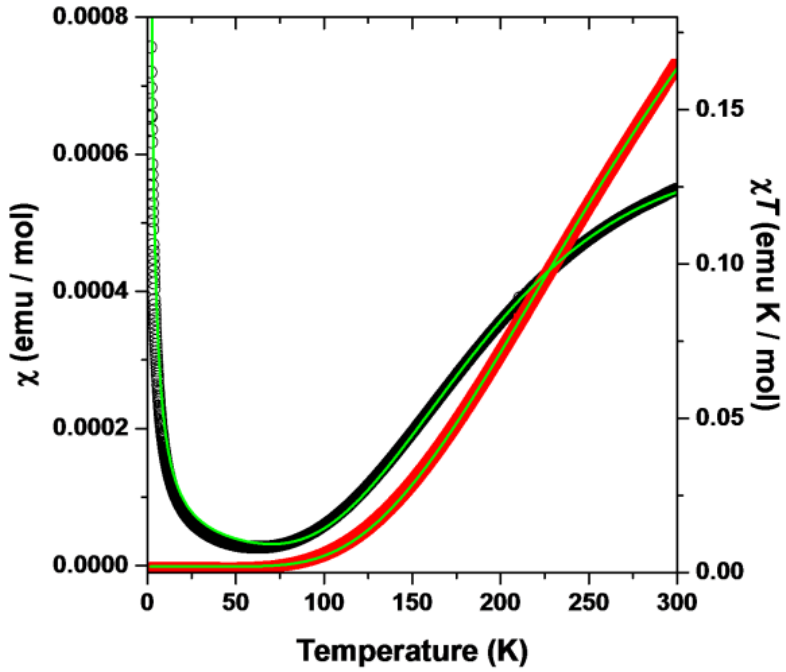

Figure S17: χT *vs*. *T* (red squares) and χ *vs*. *T* (black circles) for complex **7** under a 5000 G dc field. The solid lines represent the best fit of the experimental data (see text).

Compounds 5 and 9

In accordance with their crystal structure, compounds **5** and **9** behave as isolated complexes. The decrease of χT at low temperature is due to weak intermolecular antiferromagnetic coupling.

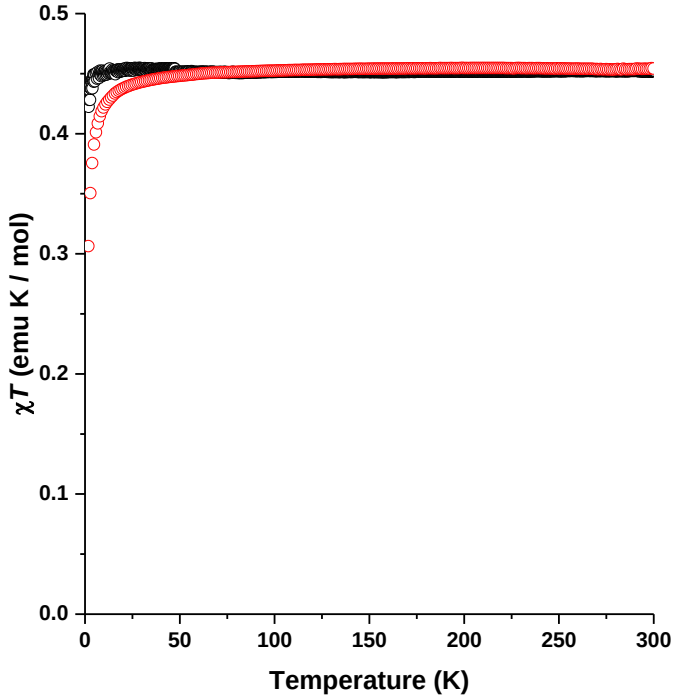

Figure S18: χT *vs. T* for complexes **5** (red) and **9** (black) under a 5000 G dc field.

Compound 6

6 exhibits antiferromagnetic behaviour. Considering its structure, its magnetic properties were fitted using the model developed by Bonner and Fisher for regular antiferromagnetic S=1/2 spin chains.[3]

Considering the following spin Hamiltonian:

$$H = -J \sum_i S_i S_{i+1}$$

the numerical expression for the susceptibility is:

$$\chi = \frac{Ng^2\beta^2}{kT} \frac{0.25 + 0.074975x + 0.075235x^2}{1.0 + 0.9931x + 0.172135x^2 + 0.757825x^3}$$

$$\text{Where } x = \frac{|J|}{kT}$$

Fitting was performed simultaneously on χT and χ, and resulted in values of g = 2.18(1) and J = -1.47(5) cm^{-1}, with $R = 4\times10^{-4}$.

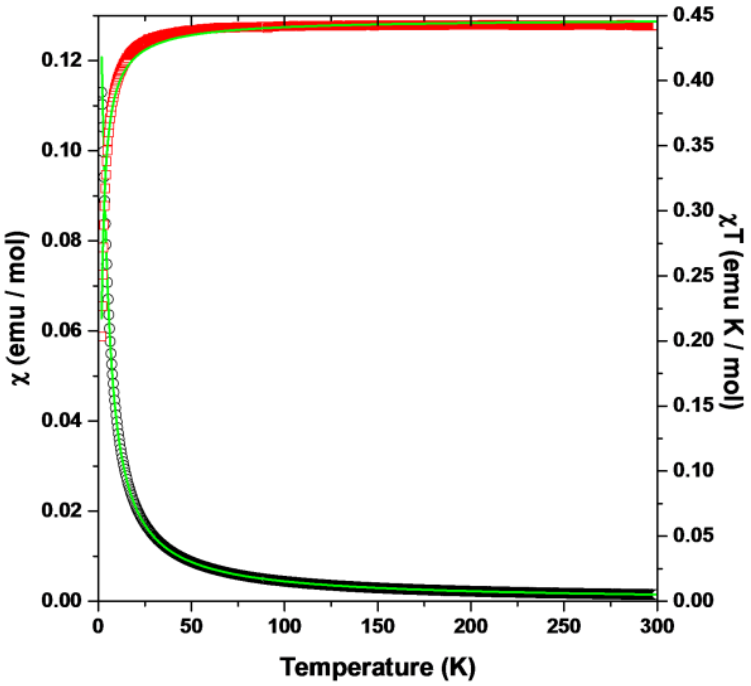

Figure S19: χT *vs.* *T* (red squares) and χ *vs.* *T* (black circles) for complex **6** under a 5000 G dc field. Solid lines represent the best fitting of the experimental data (see text).

Compound 10b

The properties of complex **10b** were fitted using an alternating chain, with two alternating magnetic interactions between the spin carriers, J_1 and J_2. [4] The actual structure of **10b** consisted of end-on azido bridged copper (II) dimers linked by carboxylate bridges. The very small Cu-N-Cu angles suggested a most probably ferromagnetic interaction (Figure S21) between the azido-bridged Cu(II) ions, [5] (although there is one previous report describing asymmetric end-on azide bridged copper(II) complexes for which an antiferromagnetic coupling is observed[6]). In the present case, the best fit was obtained considering an F/AF alternating chain, with g = 2.24(1), J_1 = -1.62(5) cm^{-1} and J_2 = 1.17(5) cm^{-1} with R = 2×10^{-4}.

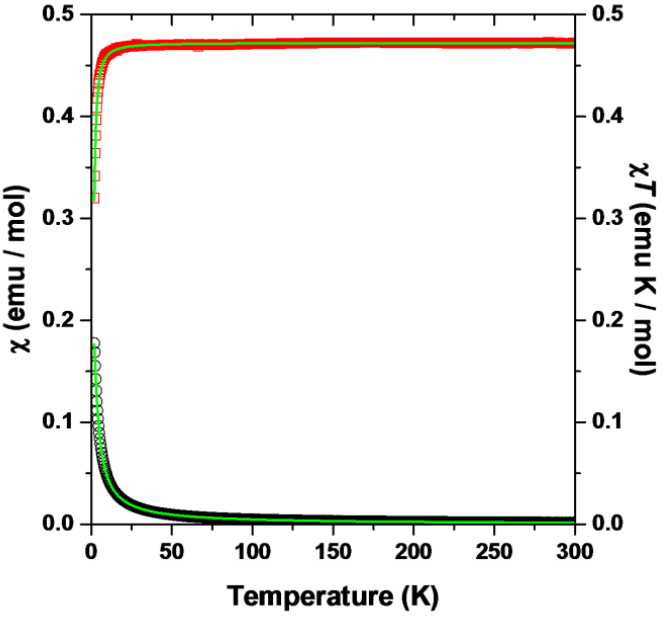

Figure S20: χT *vs.* *T* (red squares) and χ *vs.* *T* (black circles) for complex **10b** under a 5000 G dc field. Solid lines represent the best fitting of the experimental data (see text).

Compound 11

Compound **11** presents a weak ferromagnetic interaction between spin carriers. The magnetic behaviour of **11** was thus fitted using the high temperature expansion series proposed by Baker *et al.*[7] (Figure S22). At low temperatures, the product χT decreases with decreasing temperature because of interchain antiferromagnetic interactions. The fit was thus performed for temperatures above 20 K, and produced the values g = 2.26(5) and J = 0.2(1) cm^{-1}, with $R = 1 \times 10^{-5}$.

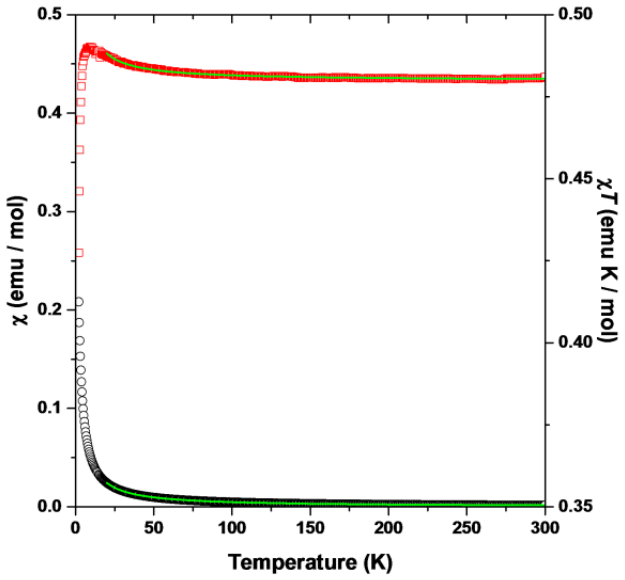

Figure S21: χT *vs. T* (red squares) and χ *vs. T* (black circles) for complex **11** under a 5000 G dc field. Solid lines represent the best fitting of the experimental data (see text).

Preliminary relaxivity measurements

All T_1 values were measured using an Agilent DDR2 500 MHz spectrometer (11.7 T) using an inversion-recovery procedure. The acquisition time, relaxation delay and the number of scans acquired were optimized for each sample. Samples were measured in a 60 µL of D_2O in a coaxial NMR tube insert (Wilmad glass) with PBS inside a 5 mm NMR tube containing d_6-DMSO.

The efficiency of the copper (II) complexes to improve the contrast in magnetic resonance images was gauged by their longitudinal relaxivity r_1 (see table 1). r_1 represents the paramagnetic relaxation enhancement of the longitudinal relaxation rate of the water protons as a result of the interaction with the paramagnetic complexes at a given temperature and magnetic field:

$$r_1 = \left(\frac{1}{T_{1,obs}} - \frac{1}{T_{1,di}}\right)[Cu^{II}]^{-1}$$

Where $T_{1,\text{observed}}$ is the longitudinal relaxation time and $T_{1,\text{diamagentic}}$ is the relaxation time in the absence of the complexes (15.39 s for D_2O at rt and 3.09 s for PBS/ d_6-DMSO at 37 °C).

Table S1. T_1 and relaxivity values of complexes **5, 6, 9, 10b** and **11** (preliminary measurements at 500 MHZ/11.7 T) at a concentration of 10 mM.

Complexes	**T_1[a] (s)**	**r_1[a] ($mM^{-1}\,s^{-1}$)**
5	0.1983	0.5164
6	0.2858	0.3347
9	0.7494	0.1575
10b	0.3766	0.2441
11	0.3673	0.2497

[a] Relaxation time and relaxivity values were obtained from copper complexes in D_2O at room temperature.

Preclinical relaxivity measurements

T_1-weighted MR images and T_1 relaxivities were measured using a conventional spin−echo acquisition in a 500 MHz Agilent preclinical MR system (9.4 T, 160 mm bore, actively screened) at room temperature. PBS solutions of complexes **5** and **6** with different molar concentrations of Cu(II) (0.1, 0.2, 0.4, 0.6, 0.8, 1.0, 10, 20, 30, 40, 50 mM) were prepared in 5.0 mL syringes. MR images were obtained using the SE/2D sequence; four echoes were employed with the following parameters: FOV = 19.2 cm, matrix = 192 × 192, TE = 16 ms, and TR = 70 ms.

Figure S22. T_1-weighted MR images for complex **5**

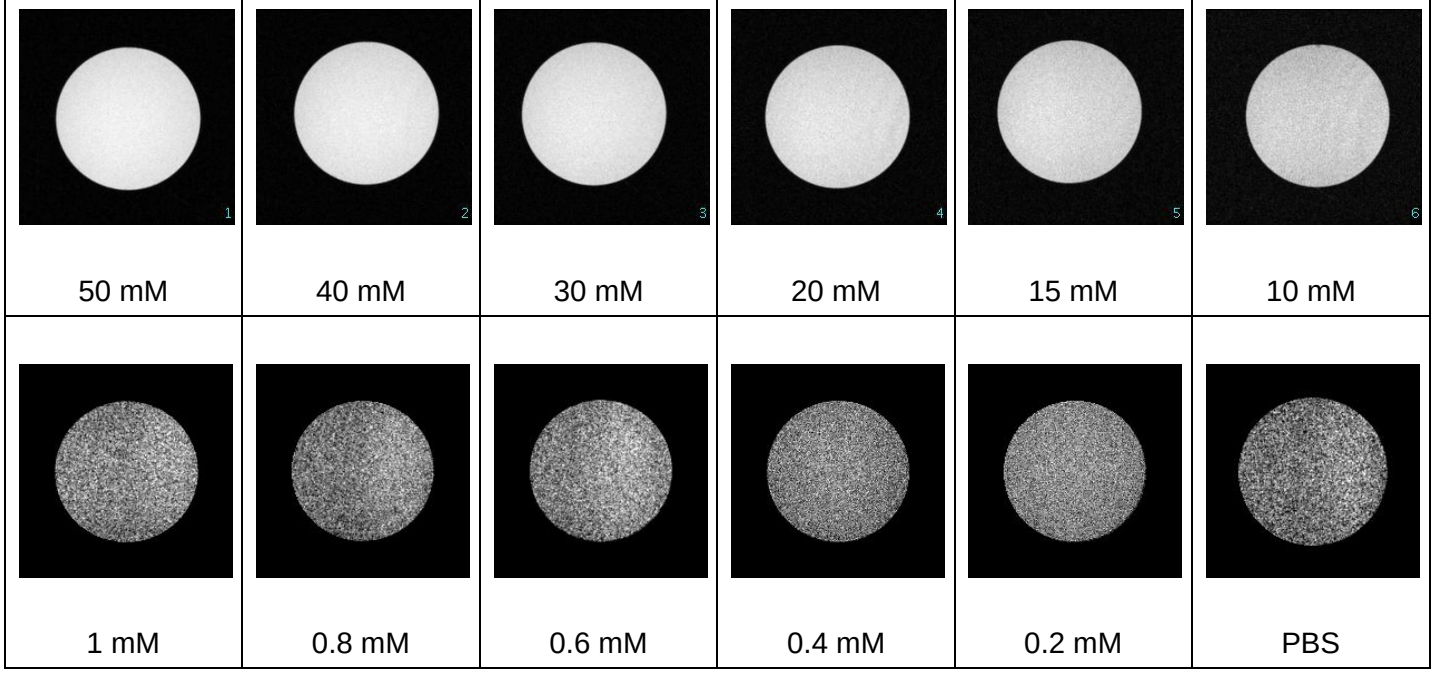

Figure S23. T_1-weighted MR images for complex **6**

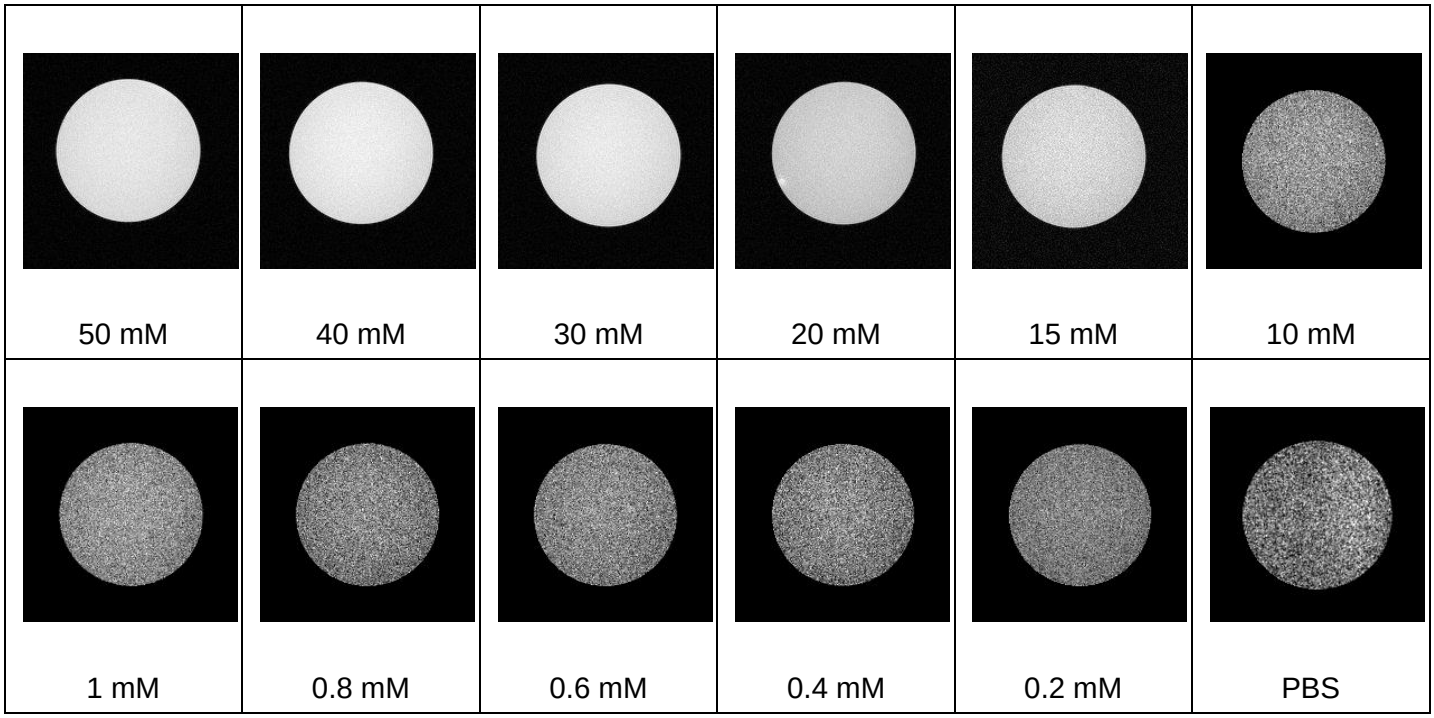

Cytotoxicity/cell proliferation assay

Cell viability was evaluated using the 3-[4,5-dimethylthiazol-2-yl]-2,5-diphenyl tetrazolium bromide or MTT assay (Sigma Aldrich). CHO and HELA cells seeded on 96-well plates were treated with solutions of the copper compounds in PBS diluted in growth medium to a final concentration of 0.1, 1, 10, 25, 50 or 100 µM, or with growth medium alone (controls) for 48 h. The growth medium was then removed and 100 µL per well of yellow MTT solution (0.5 mg ml^{-1} in PBS) was added and incubated for 3 h. Afterwards, the cells were washed twice with 100 µL of PBS. The purple formazan crystals formed in the cells after the cleavage of the tetrazolium ring by the mitochondrial dehydrogenases of viable cells were dissolved in 100 µL of DMSO. Absorbance was measured using a 96-well plate reader at 570 nm and was corrected by subtracting the absorbance at 690 nm as a background.

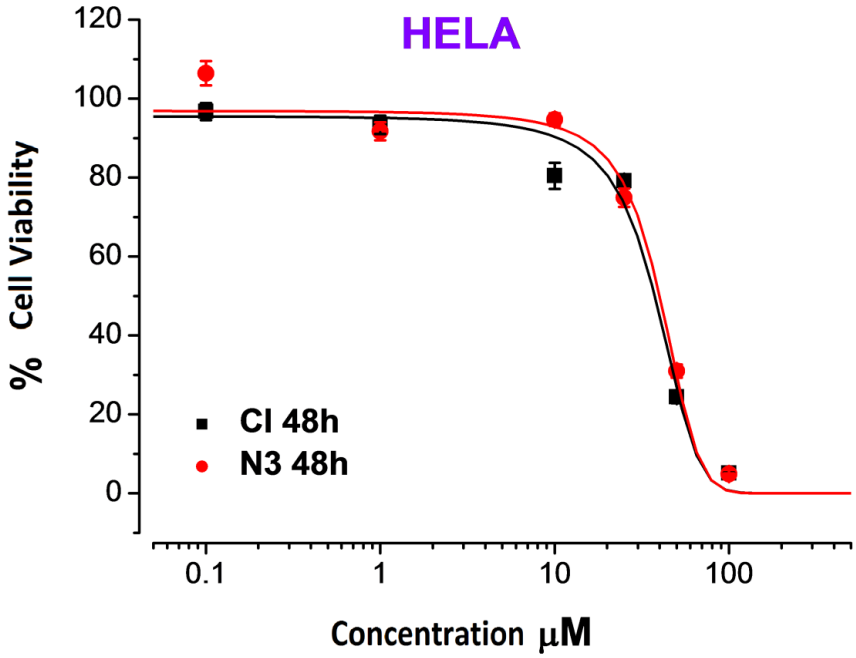

Figure S24: Treatment of HELA cells with complexes **5** and **7b** showed a cytotoxic effect in a concentration-dependent manner. The cell viability was measured after 48 h by MTT assay.

The IC_{50} values (*i.e.* the concentration of the complex that restricts cell growth to 50% of that compared with the control) were calculated from curves constructed by plotting cell survival (%) *versus* compound concentration (µM). It was found that the complexes exhibited concentration-dependent cytotoxic activity in a concentration-dependent manner; these values are given in Table S2.

Table S2. IC_{50} values of the copper complexes

Cell line	Complex 5	Complex 7
CHO	42.74 µM ± 3.99	13.06 µM ± 1.41
HELA	37.55 µM ± 2.35	40.05 µM ± 2.18

Table S3. Crystallographic data

	1b	**2b**	**4[β-ala]**	**5**
Formula	$C_{14}H_{14}Cl_4Cu_2N_2O_2$	$C_{14}H_{14}N_2O_2Cl_2Cu$	$C_{13}H_{19}N_3O_4Cl_2Cu$	$C_9H_{12}Cl_2CuN_2O_3$
M_f	511.15	376.71	415.75	330.65
crystal system	triclinic	triclinic	triclinic	monoclinic
space group	P-1	P-1	P-1	P21/n
a [Å]	7.9027(15)	7.5026(8)	8.0134(6)	8.8843(4)
b [Å]	8.1307(16)	7.5541(9)	8.7640(7)	14.8928(5)
c [Å]	8.3402(18)	8.0228(10)	13.5581(10)	10.1346(4)
α [º]	103.091(17)	98.797(10)	71.195(7)	90.00
β [º]	111.393(18)	110.504(11)	80.719(6)	111.485(5)
γ [º]	107.507(17)	109.976(10)	66.268(8)	90.00
V [Å^3]	440.43(17)	380.59(9)	824.59(13)	1247.76(10)
Z	1	1	2	4
ρ [Mgm^{-3}]	1.927	1.644	1.674	1.760
μ(Mo Kα) [mm^{-1}]	3.030	1.789	1.670	2.175
crystal size [mm]	0.3988 × 0.3608 × 0.1896	0.2398 × 0.1713 × 0.0986	0.3468 × 0.1971 × 0.1384	0.1999 × 0.1625 × 0.0821
F(000)	254.0	191.0	426.0	668.0
2θ range [º]	5.668 to 57.064	5.702 to 57.478	5.298 to 57.228	5.12 to 57.22
Max./min. transmission	0.540/0.270	0.752/0.575	0.844/0.726	0.856/0.725
reflns collected	2813	2393	5267	5007
indep. refl. [R(int)]	1972 [0.0287]	1696 [0.0157]	3682 [0.0199]	2804 [0.0185]
GOF on F^2	1.036	1.074	1.069	1.047
parameters/restraints	0/110	0/98	0/225	158/0
R_1 (on F, $I > 2\sigma$ (I))	0.0430	0.0352	0.0372	0.0388
wR_2(on F^2, all data)	0.0997	0.0792	0.0883	0.0868
Max/min $\Delta\rho$ [eÅ^{-3}]	0.42/-0.48	0.47/-0.27	0.39/-0.39	0.37/-0.38
CCDC number	1955683	1955681	1955682	1491835

	6	**7**	**8**	**9**
Formula	$C_9H_9ClCuN_2O_2$	$C_7H_8ClCuNO_2$	$C_{30}H_{32}Cl_4Cu_4N_4O_6$ 297.15	$C_{11}H_{13}CuN_3O_3S$
M_f	276.17	237.13	940.55	330.84
crystal system	monoclinic	monoclinic	tetragonal	monoclinic
space group	P21/c	P21/n	$P4_12_12$	P21/c
a [Å]	7.9634(8)	10.6181(5)	8.810(1)	7.8730(3)
b [Å]	9.7573(7)	4.0692(2)	8.810(1)	14.0579(6)
c [Å]	13.5662(10)	19.2298(9)	48.380(1)	12.7811(5)
α [º]	90.00	90.00	90	90.00
β [º]	103.354(9)	95.417(4)	90	93.857(4)
γ [º]	90.00	90.00	90	90.00
V [Å^3]	1025.61(14)	827.15(7)	3755.1(2)	1411.38(10)
Z	4	4	4	4
ρ [Mgm^{-3}]	1.789	1.904	1.664	1.557
μ(Mo Kα) [mm^{-1}]	2.368	2.915	2.564	1.701
crystal size [mm]	0.2302 × 0.1247 × 0.1101	0.3014 × 0.0974 × 0.058	0.168 × 0.165 × 0.091	0.2069 × 0.157 × 0.0687
F(000)	556.0	476.0	1888.0	676.0
2θ range [º]	5.2 to 58.86	4.22 to 56.8	4.7 to 57.304	4.32 to 57.32
Max./min. transmission	0.824/0.721	0.860/0.666	1/0.924	0.911/0.726
reflns collected	5162	3121	9186	5953
indep. refl. [R(int)]	2423 [0.0231]	1840 [0.0328]	4283[0.0363]	3187 [0.0306]
GOF on F^2	1.015	1.086	1.196	0.909
parameters/restraints	136/0	110/0	0/220	176/3
R_1 (on F, $I > 2\sigma(I)$)	0.0350	0.0440	0.0604	0.0438
wR_2(on F^2, all data)	0.0822	0.1091	0.1353	0.1524
Max/min $\Delta\rho$ [eÅ^{-3}]	0.65/-0.55	0.54/-0.35	0.46/-0.40	0.89/-0.65
CCDC number	1491837	1491836	1955678	1491838

	10a	**10b**	**11**
Formula	$C_9H_9CuN_5O_2$	$C_9H_9CuN_5O_2$	$C_{10}H_9CuN_3O_3$
M_f	282.75	282.75	282.74
crystal system	monoclinic	monoclinic	monoclinic
space group	P21/n	P21/c	P21/n
a [Å]	8.6172(3)	7.4821(4)	8.6356(3)
b [Å]	9.2484(3)	18.0234(7)	9.5813(3)
c [Å]	14.1381(5)	7.8559(3)	13.5642(4)
α [º]	90.00	90.00	90.00
β [º]	107.055(4)	98.848(5)	106.101(3)
γ [º]	90.00	90.00	90.00
V [Å^3]	1077.19(6)	1046.78(8)	1078.29(6)
Z	4	4	4
ρ [Mgm^{-3}]	1.744	1.794	1.742
μ(Mo K□) [mm^{-1}]	2.025	2.083	2.024
crystal size [mm]	0.3675 × 0.2176 × 0.1224	0.2255 × 0.089 × 0.028	0.353 × 0.2863 × 0.128
F(000)	572.0	572.0	572.0
2θ range [º]	4.98 to 59.44	4.52 to 57.1	5.04 to 57.5
Max./min. transmission	0.824/0.670	0.944/0.669	0.801/0.630
reflns collected	5732	4420	4505
indep. refl. [R(int)]	2565 [0.0240]	2351 [0.0445]	2411 [0.0212]
GOF on F^2	0.856	1.018	1.060
parameters/restraints	154/3	154/3	154/3
R_1 (on F, $I > 2\sigma(I)$)	0.0328	0.0544	0.0342
wR_2(on F^2, all data)	0.1225	0.1035	0.0861
Max/min $\Delta\rho$ [eÅ^{-3}]	0.37/-0.39	0.46/-0.36	0.39/-0.27
CCDC number	1491839	1491840	1491841

1 1 S. Boonlue, A. Sirikulkajorn and K. Chainok, *Acta Crystallographica Section* E, 2015, **71**, m44-m45.
2 a) M. Kato and Y. Muto, *Coord. Chem. Rev*., 1988, **92**, 45-83; b) M. Melník, *Coord. Chem. Rev*., 1982, **42**, 259-293; c) V. H. Crawford, H. W. Richardson, J. R. Wasson, D. J. Hodgson and W. E. Hatfield, *Inorg. Chem*., 1976, **15**, 2107-2110; d) W. Plass, A. Pohlmann and J. Rautengarten, *Angew. Chem. Int. Ed*., 2001, **40**, 4207-4210.
3 a) J. C. Bonner and M. E. Fisher, *Phys. Rev. A*, 1964, **135**, 640; b) W. E. Estes, D. P. Gavel, W. E. Hatfield and D. Hodgson, *Inorg. Chem*., 1978, **17**, 1415; c) O. Kahn, Molecular Magnetism, Wiley VCH, 1993**.**
4 a) W. Duffy and K. P. Barr, *Phys. Rev*., 1968, **165**, 647; b) J. W. Hall, W. E. March, R. R. Weller and W. E. Hatfield, *Inorg. Chem*., 1981, **20**, 1033; c) R. Georges, J. J. Borrás-Almenar, E. Coronado, J. Curély and M. Drillon, *In Magnetism: Molecules to Materials. Models and Experiments,* Eds. Wiley-VCH, Weinheim, 2001, p 1-47.
5 a) S. Mukherjee and P. S. Mukherjee, *Acc. Chem. Res.,* 2013, **46**, 2556-2566; b) C. Adhikary and S. Koner, *Coord. Chem. Rev.,* 2010, **254**, 2933-2958.
6 S. Koner, S. Saha, T. Mallah and K.-I. Okamoto, *Inorg. Chem.,* 2004, **43**, 840-842.
7 G. A. Baker Jr., G. S. Rushbrooke and H. E. Gilbert, *Phys. Rev*., 1964, **135**, A1272.